Simple analytical solutions for under-ground circular, elliptical and rectangular openings

Author: Prof. Dr. habil. Heinz Konietzky
(TU Bergakademie Freiberg, Geotechnical Institute)

1   Introduction

Over the last decades and centuries a lot of analytical solutions were obtained for elastic, elasto-plastic, visco-elastic and visco-elasto-plastic problems with simple geometry. Some of them, especially those with openings (holes) in the 2-dimensional half space or infinite space allow to estimate the stress-strain situation for geotechnical structures (circular tunnels, shafts, drifts, boreholes etc.). Exemplary, this chapter gives a few very simple 2-dimensional analytical solutions.

For some of the 2D solutions a polar coordinate system (fig. 1) is more suitable compared to a Cartesian, although solutions are available for both of them. The transformation of stresses between Cartesian (x-y-system) and polar (r-φ-system) coordinates is given by eq. 1 and illustrated by fig. 1.

$$\sigma_r = \frac{1}{2}\left(\sigma_x + \sigma_y\right) + \frac{1}{2}\left(\sigma_x - \sigma_y\right)\cos 2f + \tau_{xy}\sin 2f$$

$$\sigma_f = \frac{1}{2}\left(\sigma_x + \sigma_y\right) - \frac{1}{2}\left(\sigma_x - \sigma_y\right)\cos 2f + \tau_{xy}\sin 2f$$

$$\tau_{rf} = -\frac{1}{2}\left(\sigma_x - \sigma_y\right)\sin 2f + \tau_{xy}\cos 2f$$

$$(1)$$

Also, in 2D we can distinguish between

- plane stress: $\sigma_z = \tau_{xz} = \tau_{yz} = 0$ and $\varepsilon_z = -\frac{v}{E}\times\left(\sigma_x + \sigma_y\right)$ and

- plane strain: $\varepsilon_z = \gamma_{xz} = \gamma_{yz} = 0$ and $\sigma_z = v(\sigma_x + \sigma_y)$ if we consider the x-y-plane.

Assuming that the considered plane is the x-y-plane and the z-axis is perpendicular to the x-y-plane, the following holds:

Plane stress:
$$\sigma_{ij} = \begin{bmatrix} \sigma_{xx} & \sigma_{xy} & 0 \\ \sigma_{yx} & \sigma_{yy} & 0 \\ 0 & 0 & 0 \end{bmatrix} \text{ and } \varepsilon_{ij} = \begin{bmatrix} \varepsilon_{xx} & \varepsilon_{xy} & 0 \\ \varepsilon_{yx} & \varepsilon_{yy} & 0 \\ 0 & 0 & \varepsilon_{zz} \end{bmatrix} \quad (2)$$

Plane strain
$$\sigma_{ij} = \begin{bmatrix} \sigma_{xx} & \sigma_{xy} & 0 \\ \sigma_{yx} & \sigma_{yy} & 0 \\ 0 & 0 & \sigma_{zz} \end{bmatrix} \text{ and } \varepsilon_{ij} = \begin{bmatrix} \varepsilon_{xx} & \varepsilon_{xy} & 0 \\ \varepsilon_{yx} & \varepsilon_{yy} & 0 \\ 0 & 0 & 0 \end{bmatrix} \quad (3)$$

Considering the Boltzmann-Axiom (momentum equilibrium) the following holds:
$\sigma_{xy} = \sigma_{yx}$ and $\varepsilon_{xy} = \varepsilon_{yx}$

Quite often the horizontal principal stress q is given as a fraction of the principal vertical stress component *p*, whereby $q = \lambda p$. λ is also called lateral earth pressure coefficient (see fig. 2).

Simple analytical solutions for underground circular, elliptical and rectangular openings

Only for private and internal use!   Updated: 22 February 2022
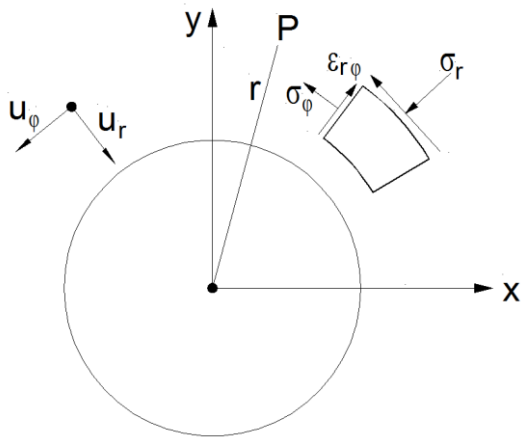

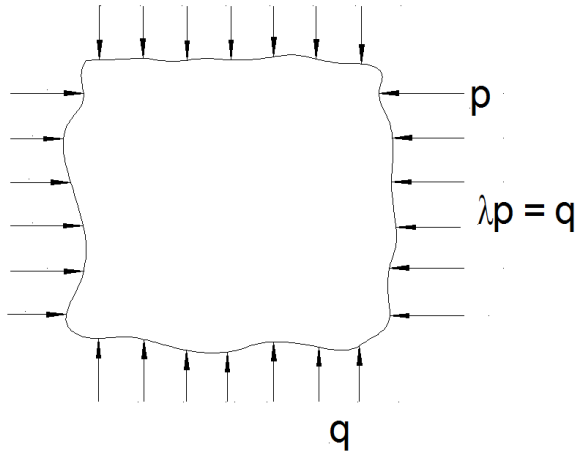Fig. 1: Illustration of physical units in polar coordinates.

Fig.2: Sketch for virgin stress field (far-field stresses)

The anisotropic far-field stress state (virgin or primary stresses) is given by the following equations using a polar coordinate system:

$$\overset{o}{\sigma}_r = \frac{p}{2}\left\{(1+\lambda)-(1-\lambda)\cos 2\varphi\right\}$$

$$\overset{o}{\sigma}_\phi = \frac{p}{2}\left\{(1+\lambda)+(1-\lambda)\cos 2\varphi\right\} \tag{4}$$

$$\overset{o}{\tau}_{r\phi} = \frac{p}{2}(1-\lambda)\sin 2\varphi$$

In Cartesian coordinates the far-field stresses are: $\overset{o}{\sigma}_x = \lambda p$, $\overset{o}{\sigma}_y = p$ and $\overset{o}{\tau}_{xy} = 0$.

2   Analytical solutions in 2D

2.1   Internal hydrostatic pressure

Hydrostatic pressure q inside a circular opening of radius a induces a radial symmetric stress field with two principal stress components (radial and tangential stresses):

$$\sigma_r = q\frac{a^2}{r^2} \quad \text{and} \quad \sigma_\varphi = -q\frac{a^2}{r^2} \tag{5}$$

Simple analytical solutions for underground circular, elliptical and rectangular openings

Only for private and internal use!   Updated: 22 February 2022

The variable r ($r \geq a$) measures the distance from the centre of the opening. At the boundary of the opening ($r = a$) the stresses reach maximum values: compression of magnitude q as radial stress and tension of magnitude $-q$ as tangential stress.

2.2   Circular opening in infinite elastic space and anisotropic stress field

The elastic stress field around a circular opening is given by the so-called Kirsch-solution, which considers an anisotropic far-field stress state, characterized by λ. Figure 4 illustrates the situation and Eq. 6 gives the corresponding equations for radial, tangential and shear stresses.
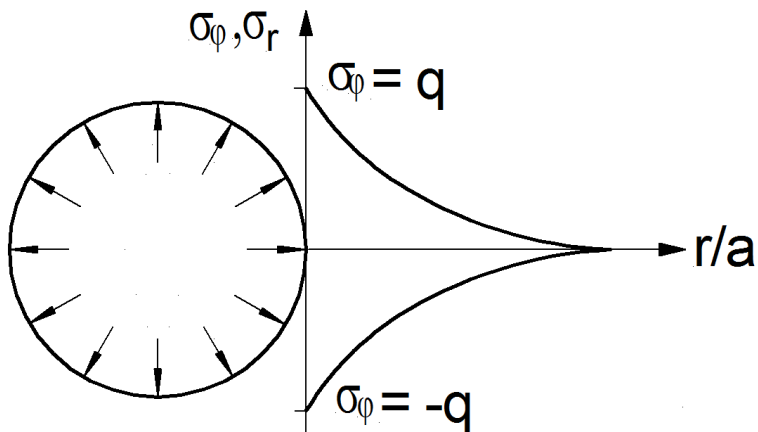

Fig. 3: Illustration of stress field around circular opening under internal hydrostatic pressure.
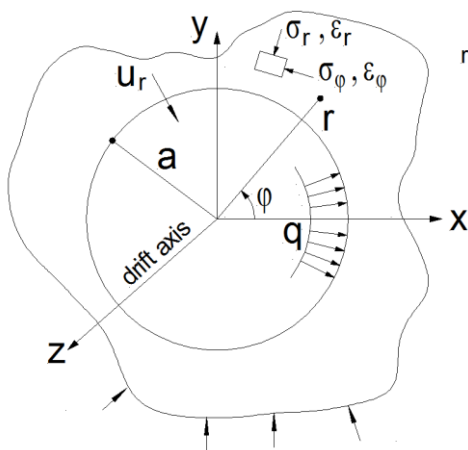

Fig. 4: Geometrical model of circular hole in an anisotropic infinite space

$$\sigma_r = \frac{p}{2}\left[(1+\lambda)\left(1-\frac{a^2}{r^2}\right)-(1-\lambda)\left(1-4\frac{a^2}{r^2}+3\frac{a^4}{r^4}\right)\cos 2\varphi\right]$$

$$\sigma_\varphi = \frac{p}{2}\left[(1+\lambda)\left(1+\frac{a^2}{r^2}\right)+(1-\lambda)\left(1+3\frac{a^4}{r^4}\right)\cos 2\varphi\right] \qquad (6)$$

$$\tau_{r\varphi} = \frac{p}{2}\left[(1-\lambda)\left(1+2\frac{a^2}{r^2}-3\frac{a^4}{r^4}\right)\sin 2\varphi\right]$$

The Kirsch-solution shows an inhomogeneous and anisotropic stress field, whereby the most critical values (minimum and maximum tangential stresses) are reached at the surface of the opening (deduced by setting first derivatives of Eq. 6 to zero):

$$\sigma_\varphi(\varphi=0) = p\left[(1+\lambda)+2(1-\lambda)\right] = p(3-\lambda) \qquad (7)$$

$$\sigma_\varphi\left(\varphi=\frac{\pi}{2}\right) = p\left[(1+\lambda)-2(1-\lambda)\right] = p(3\lambda-1) \qquad (8)$$

Considering the inner pressure q (see Fig. 4) leads the following equations:

$$\sigma_\varphi(\varphi=0) = p\left[(1+\lambda)+2(1-\lambda)\right] = p(3-\lambda) - q$$

$$\qquad (7a)$$

$$\sigma_\varphi\left(\varphi=\frac{\pi}{2}\right) = p\left[(1+\lambda)-2(1-\lambda)\right] = p(3\lambda-1) - q \qquad (8a)$$

Figures 5 to 7 illustrate the stress distribution around the opening in form of different diagrams.
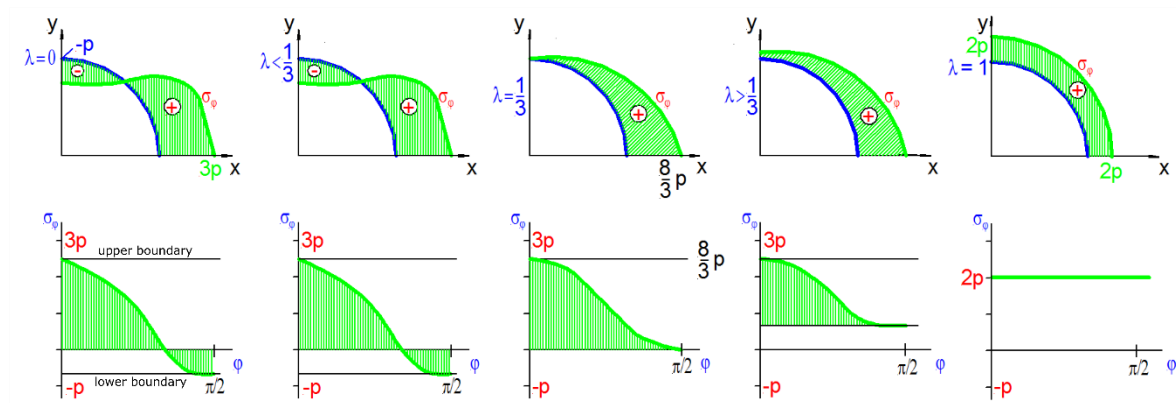
Fig. 5: Tangential stresses σ_φ along the boundary of the opening for different values of λ.

Simple analytical solutions for underground circular, elliptical and rectangular openings

Only for private and internal use!   Updated: 22 February 2022
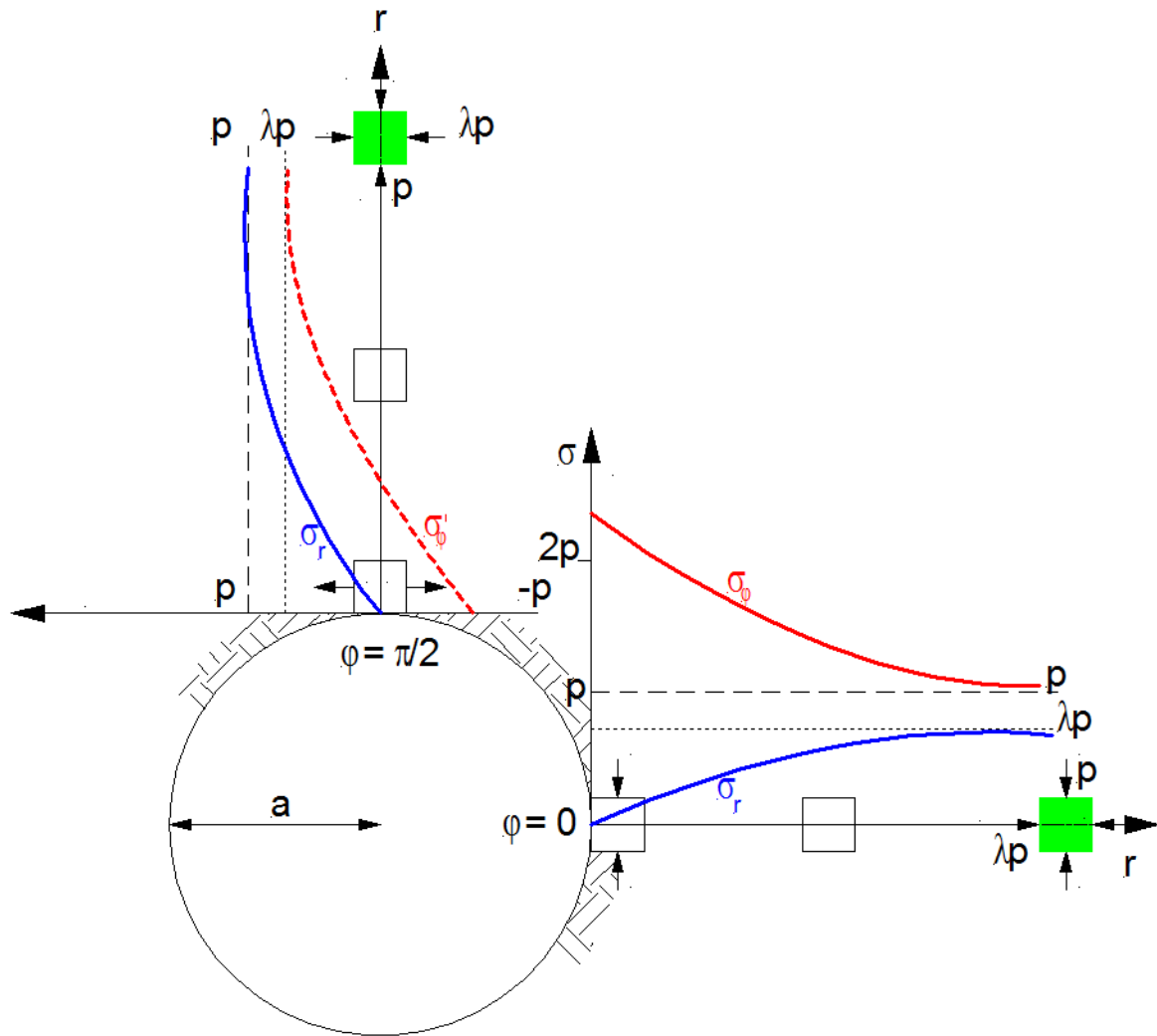
Fig. 6: Principal stress pathway for two selected points with extreme values.
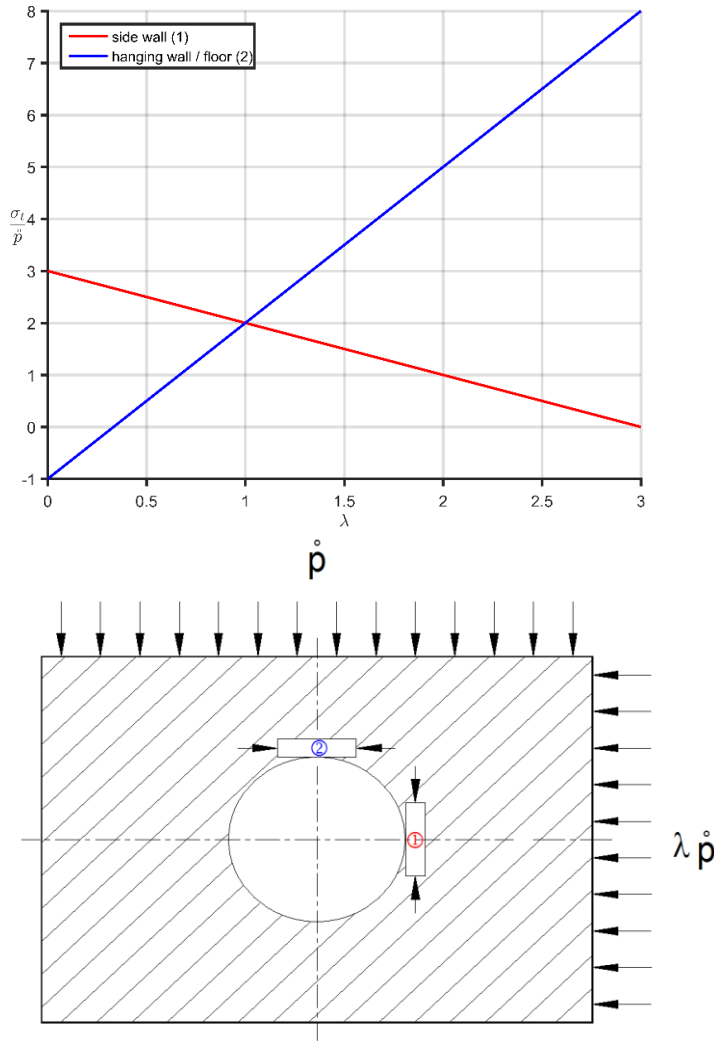
Fig. 7: Scaled tangential stresses vs. earth pressure coefficient at locations of extreme values

Induced radial and tangential displacements at the boundary of the opening ($r = a$) are given by Eq. 9 and 10.

$$\Delta u_r (r = a) = \frac{pa}{4\dfrac{E}{1+\nu}} 2(w+1)\left[(1+\lambda) - 2(1-\lambda)\cos 2\varphi\right] \tag{9}$$

$$\Delta u_\varphi (r = a) = \frac{pa}{4\dfrac{E}{1+\nu}} 2(w+1)(1-\lambda)\sin 2\varphi \tag{10}$$

For plain strain holds: $w = 3 - 4\nu$ and for plain stress holds: $w = \dfrac{3-\nu}{1+\nu}$. Transformation into Cartesian coordinates leads to the following expressions:

$$u_x = \frac{pa}{4E}(1+\nu)(w+1)(3\lambda - 1)\cos\varphi \tag{11}$$

$$u_y = \frac{pa}{4E}(1+\nu)(w+1)(3-\lambda)\sin\varphi \tag{12}$$

The deformations at the contour lead to an elliptical shape of the opening. If we define $u_0 = \dfrac{p \cdot a}{4E}(1+v)(w+1)$ the following expression is obtained:

$$\left.\begin{array}{l} \bar{x} = \left[a - u_0\left(3\lambda - 1\right)\right]\cos\varphi = \bar{a}\cos\varphi \\ \bar{y} = \left[a - u_0\left(3 - \lambda\right)\right]\sin\varphi = \bar{a}\sin\varphi \end{array}\right\} = \text{equation of ellipse in parameter notation} \quad (13)$$

2.2.1 Special case: Isotropic far field stresses

In case of isotropic primary stress field ($\lambda = 1$) and vanishing inner pressure the Kirsch-solution (Eq. 4) yields the following stress field (principal stress components):

$$\sigma_r = p\left(1 - \frac{a^2}{r^2}\right) \qquad (14)$$

$$\sigma_\varphi = p\left(1 + \frac{a^2}{r^2}\right) \qquad (15)$$

The obtained radial symmetric solution (stresses are independent on φ) gives maximum tangential stresses at the contour of $2p$ (see also Fig. 8).
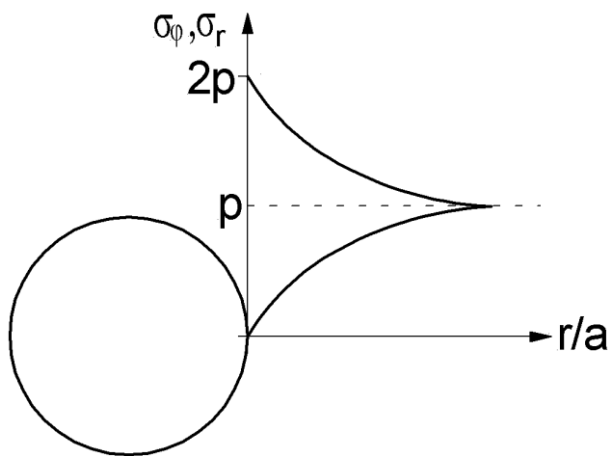

Fig. 8: Secondary stress state around a circular opening with isotropic far-field stresses of magnitude p.

Simple analytical solutions for underground circular, elliptical and rectangular openings

Only for private and internal use!   Updated: 22 February 2022
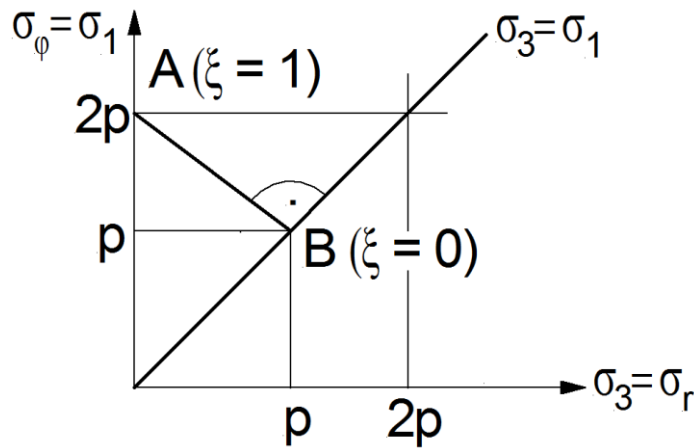

Fig. 9: Principal stress values (from B: far field - to A: boundary of opening)

Figure 9 illustrates all stress states in the principal stress diagram. Far away from the opening the virgin stress field with magnitude p is reached (point B) and at the boundary the extreme values ($2p$ and 0) are reached. Therefore, all stress states are located along the line A-B.

2.2.2 Special case: Isotropic far-field stress and hydrostatic inner pressure

Superposition principle (valid for elastic stress fields) is used to deduce stress field under consideration of isotropic far field stress p and hydrostatic pressure q at the boundary of the opening (Figure 10).

Identical extreme values are obtained all along the boundary:

$$\sigma_\varphi = 2p - q \qquad\qquad\qquad\qquad\qquad\qquad\qquad\qquad (16)$$
$$\sigma_r = q \qquad\qquad\qquad\qquad\qquad\qquad\qquad\qquad\qquad\qquad (17)$$

Figure 12 illustrates all stress states in the principal stress diagram. Far away from the opening the virgin stress field with magnitude p is reached (point B) and at the boundary the extreme values ($2p - q$ and q) are reached. Therefore, all stress states are located along the line A-B.
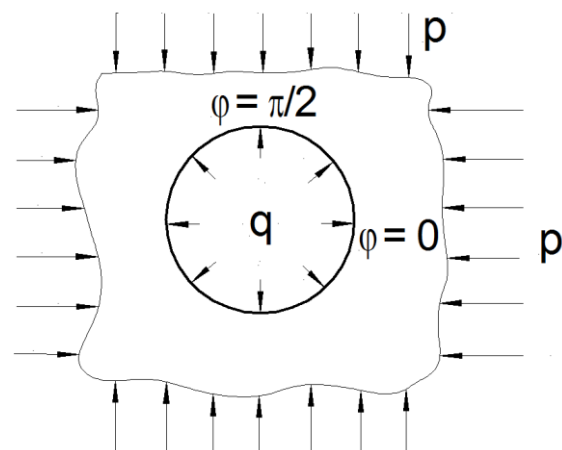
Fig. 10: Circular hole under anisotropic far-field stress and hydrostatic inner pressure

Simple analytical solutions for underground circular, elliptical and rectangular openings

Only for private and internal use!   Updated: 22 February 2022

Fig. 11: Principal stress components versus distance from boundary of opening

Fig. 12: Principal stress values (from B: far field to A: boundary of opening) in principal stress diagram

2.3   Cylindrical tube under inner and outer hydrostatic pressure

The so-called Lame-formulae describes the pressure distribution inside a tube with inner radius *a* and outer radius *b* under superimposed inner and outer hydrostatic pressure (Figure 12):

$$\sigma_r = q\frac{a^2}{r^2} + \frac{b^2 p - a^2 q}{b^2 - a^2}\left(1 - \frac{a^2}{r^2}\right) \tag{18}$$
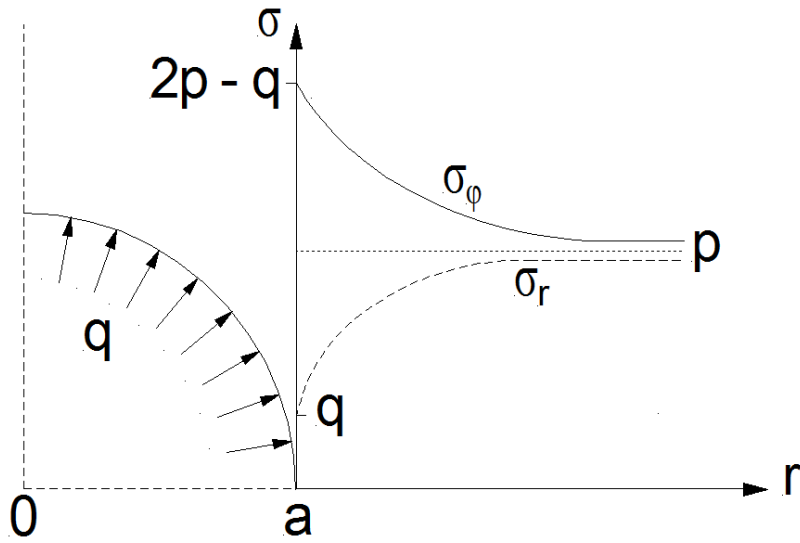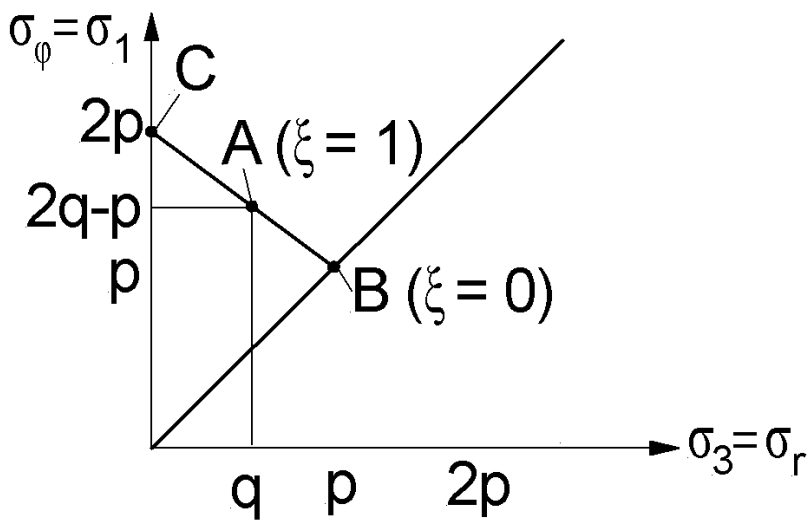
$$\sigma_\varphi = -q\frac{a^2}{r^2} + \frac{b^2 p - a^2 q}{b^2 - a^2}\left(1 + \frac{a^2}{r^2}\right) \tag{19}$$

Several special cases can be deduces if *a* and/or *b* attain extreme values (0 or ∞).

2.4   Elliptical opening in infinite elastic space

The tangential stress σ_t at the contour along an elliptical opening is given by the so-called Inglis-solution (see also Fig. 13). This solutions requires, that main axis of ellipse coincide with principal stress axes.

$$\frac{\sigma_t}{p} = \frac{2f + (1-\lambda)\left[f^2 - (1+f)^2 \sin^2\beta\right]}{f^2 + (1-f^2)\sin^2\beta} \tag{20}$$

The following geometrical relations hold:

$$\tan\varphi = \frac{y}{x} = \frac{\eta}{\xi} = f\tan\beta, \quad \text{with } \xi = \cos\beta, \ \eta = f\sin\beta \quad \text{and } f = \frac{b}{a} \tag{21}$$
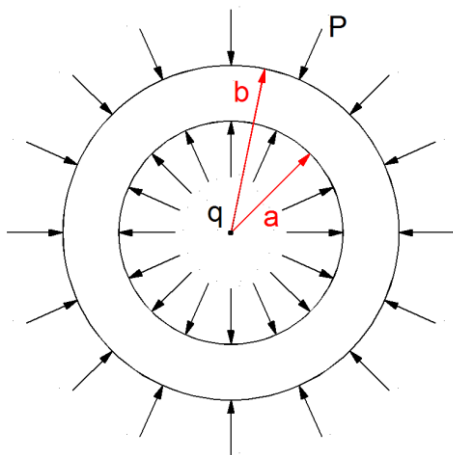

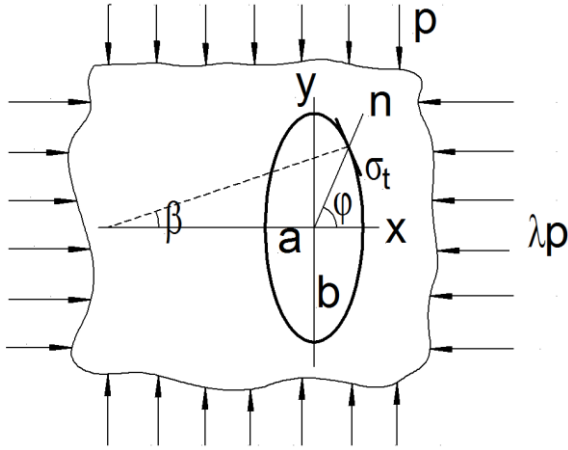Fig. 12: Illustration of Lame formulae

Fig. 13: Sketch of elliptical opening in an infinite medium

Extreme values for stresses are obtained at $\beta = 0$ and $\beta = \dfrac{\pi}{2}$:

$$\sigma_t(\beta = 0) = \frac{(1-\lambda)f + 2}{f}\, p \tag{22}$$

$$\sigma_t\left(\beta = \frac{\pi}{2}\right) = \left[(2f+1)\lambda - 1\right]p \tag{23}$$

The potential transition between compression and tension for tangential stresses is located at β_0 :

$$\sin^2 \beta_0 = \frac{2f + (1-\lambda)f^2}{(1-\lambda)(1+f)^2} \tag{24}$$

Two special cases are interesting from the engineering point of view:

$$1)\quad f = \frac{1}{\lambda} \text{ or } \lambda = \frac{1}{f}: \text{ this leads to } \sigma_t = (1+\lambda)p = const. \tag{25}$$

$$2)\quad \lambda = \frac{1}{2f+1} \text{ or } f = \frac{1-\lambda}{2\lambda}: \text{ this leads to } \sigma_t\left(\frac{\pi}{2}\right) = 0. \tag{26}$$

The first mentioned special case is called 'pressure ellipse' and provides the smallest possible compression along the contour. The second special case is called 'Fenner-ellipse' and describes the situation, where the minimum tangential stress reaches zero. Fig. 14 shows the tangential stresses at the boundary for the two locations with extreme values assuming different axis ratios f.
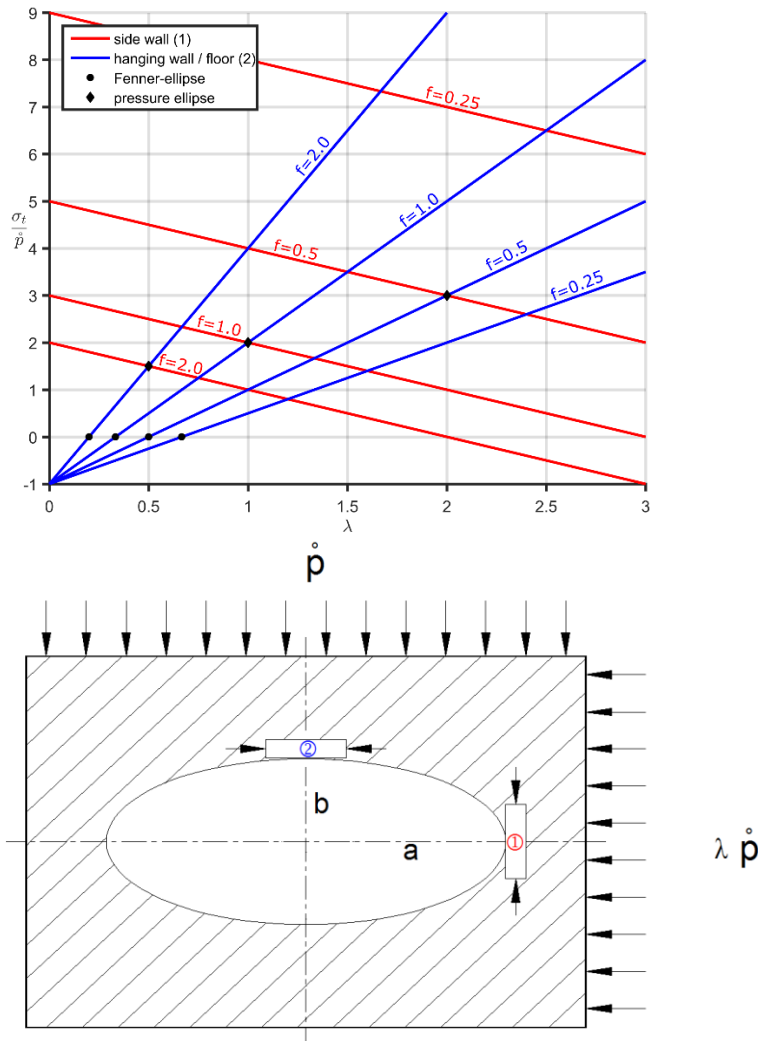
Fig. 14: Scaled tangential stresses at contour of elliptical opening with different elliptical axis ratio vs. earth pressure coefficient

The Inglis-solution can be extended by additional consideration of internal hydrostatic pressure using the superposition principle.

The tangential pressure at the contour of an elliptical opening under hydrostatic inner pressure q is given by the following expression:

$$\overset{o}{\sigma}_t = q - \frac{2f}{f^2 + \left(1 - f^2\right)\sin^2 \beta} \cdot q = \frac{f\left(f - 2\right) + \left(1 - f^2\right)\sin^2 \beta}{f^2 + \left(1 - f^2\right)\sin^2 \beta} q \tag{27}$$

Extreme values are obtained for $\beta = 0$ and $\beta = \dfrac{\pi}{2}$:

$$\sigma_t(0) = \left(1 - \frac{2}{f}\right)q \quad \text{and} \quad \sigma_t\left(\frac{\pi}{2}\right) = \left(1 - 2f\right)q \tag{28}$$

The superposition principle leads to the following expression for the tangential stresses along the contour of an elliptical opening under anisotropic far field stresses and internal hydrostatic stress:

Simple analytical solutions for underground circular, elliptical and rectangular openings

Only for private and internal use!   Updated: 22 February 2022

$$\sigma_t = \frac{\left[2f + \left(1 - \lambda\right)\left(f^2 - 1 + f\right)^2 \sin^2\beta\right]p + \left[f\left(f - 2\right) + \left(1 - f^2\right)\sin^2\beta\right]q}{f^2 + \left(1 - f^2\right)\sin^2\beta} \tag{29}$$

Again, extreme values are obtained for $\beta = 0$ and $\beta = \dfrac{\pi}{2}$:

$$\sigma_t(0) = \frac{(1-\lambda)f + 2}{f}p + \left(1 - \frac{2}{f}\right)q \tag{30}$$

$$\sigma_t\left(\frac{\pi}{2}\right) = \left[(2f+1)\lambda - 1\right]p + (1 - 2f)q \tag{31}$$

Constant minimum pressure along the contour is reached under the following condition:

$$q = p\frac{1 - \lambda f}{1 - f} \tag{32}$$

This leads to the 'generalized pressure ellipse', which results in the following constant magnitude for the tangential stresses along the boundary:

$$\sigma_t = \frac{\lambda - f}{1 - f}p = \frac{\lambda - f}{1 - \lambda f}q \tag{33}$$

2.5 Elasto-plastic solution for circular opening in isotropic stress field

If limit state (failure envelope) is reached, plasticity occurs, which is combined with stress-redistributions and additional plastic deformations. In the following we consider the simplest case: a circular opening in an isotropic material under isotropic far-field stress (Fig. 15).

Due to the isotropic virgin stress state, the boundary conditions and the circular opening, a rotationally symmetric solution is obtained. Certain different conditions have to be considered for the elastic and plastic part. This leads to separate equations in terms of stress and strain for the elastic and plastic part. But, due to the equilibrium conditions and the law of continuity, normal stress and radial displacements are identical at the transition between plastic and elastic part, which is located at R_0. The complete solution needs the assumption of a plasticity condition (failure criterion). We assume the well-known Mohr-Coulomb failure criterion (the superscript star indicates plastic values):

$$f = \sigma_\phi^* - \kappa\sigma_r^* - \sigma_F = 0 \tag{34}$$

where:

σ_F uniaxial compressive strength

$\kappa = (1 + \sin\varphi)/(1 - \sin\varphi)$
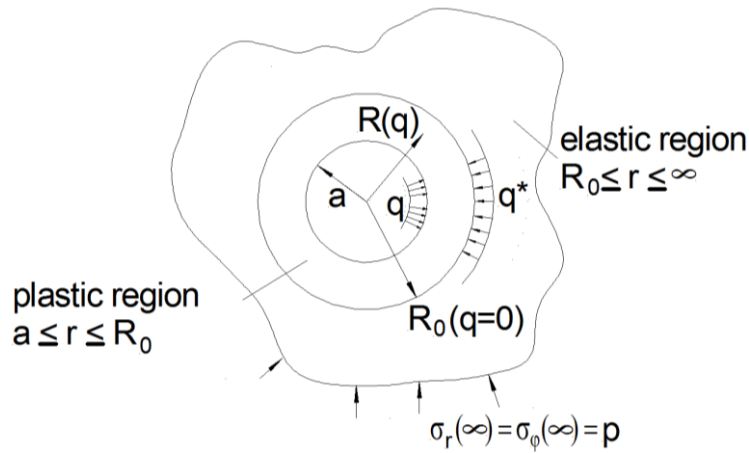
φ friction angle

Fig. 15: Sketch of circular opening with elastic and plastic part.

The extension of the plastic zone R_0 is given by the following expression:

$$\frac{R_0}{a} = {}^{(\kappa-1)}\sqrt{\frac{\kappa-1}{\kappa+1}\frac{2p-\sigma_F}{\sigma_F}+1} \tag{35}$$

The radial stress at R_0 is given by the following equation:

$$\sigma_r^*(R_0) = q^* = \frac{\sigma_F}{\kappa-1}\left[\left(\frac{R_0}{a}\right)^{\kappa-1}-1\right] = \frac{2p-\sigma_F}{\kappa+1} \tag{36}$$

Inside the elastic region ($a \geq R_0$) tangential and radial stress components are given by the following expressions:

$$\sigma_r = p-\left(p-q^*\right)\frac{a^2}{r^2} = p-\left(p-\frac{\sigma_F}{\kappa-1}\left[\left(\frac{R_0}{a}\right)^{\kappa-1}+1\right]\right)\frac{a^2}{r^2} \tag{37}$$

$$\sigma_\varphi = p+\left(p-q^*\right)\frac{a^2}{r^2} = p+\left(p-\frac{\sigma_F}{\kappa-1}\left[\left(\frac{R_0}{a}\right)^{\kappa-1}+1\right]\right)\frac{a^2}{r^2} \tag{38}$$

Inside the plastic region ($a \leq R_0$) the following equations are valid:

$$\sigma_r^* = \frac{\sigma_F}{\kappa-1}\left[\left(\frac{r}{a}\right)^{\kappa-1}-1\right] \tag{39}$$

$$\sigma_\phi^* = \frac{\kappa\cdot\sigma_F}{\kappa-1}\left[\left(\frac{r}{a}\right)^{\kappa-1}-1\right]+\sigma_F \tag{40}$$

The radial displacements inside the elastic region are given by:

Simple analytical solutions for underground circular, elliptical and rectangular openings

Only for private and internal use!   Updated: 22 February 2022

$$u_r = \frac{R_0 \cdot p}{E} \left[(1 - 2v) \frac{r}{R_0} + (1 + v) \left(1 - \frac{q^*}{p} \right) \frac{R_0}{r} \right] \tag{41}$$

Under consideration of associated plasticity (plastic potential identical to failure criterion), that means, dilation angle identical to friction angle), the radial displacements inside the plastic regions are given by the following expression:

$$u_r^* = \frac{a \cdot p}{E} \left[(1 - 2v) \frac{r}{a} + (1 + v) \frac{\kappa - 1}{\kappa + 1} \frac{a^2}{R_0^2} \cdot \frac{r}{a} + 2 \frac{1 + v}{\kappa + 1} \left(\frac{R_0}{a} \right)^{\kappa - 1} \left(\frac{a}{r} \right)^{\kappa} \right] \tag{42}$$

The radial displacements at the contour due to the creation of opening (induced displacements) are given by the following equation:

$$\Delta u_r^*(a) = \frac{a \cdot p}{E} \frac{1 + v}{\kappa + 1} \left[(\kappa - 1) \left(\frac{a}{R_0} \right)^2 + 2 \left(\frac{R_0}{a} \right)^{\kappa - 1} \right] \tag{43}$$

Fig. 16 illustrates the development of principal stress components (radial and tangential components) as function of distance from the boundary of the opening. Fig. 17 illustrates all stress states in the principal stress diagram. Far away from the opening the virgin stress field with magnitude p is reached (point A). From that point tangential stresses are increasing until they reach the absolute maximum value of $2p - q^*$ and radial stresses decrease until the reach q^* at the transition between elastic and plastic region at R_0 (point B). At the boundary (point C) the minimum values (σ_p and 0) are reached. Therefore, all stress states are located along the line A-B-C.
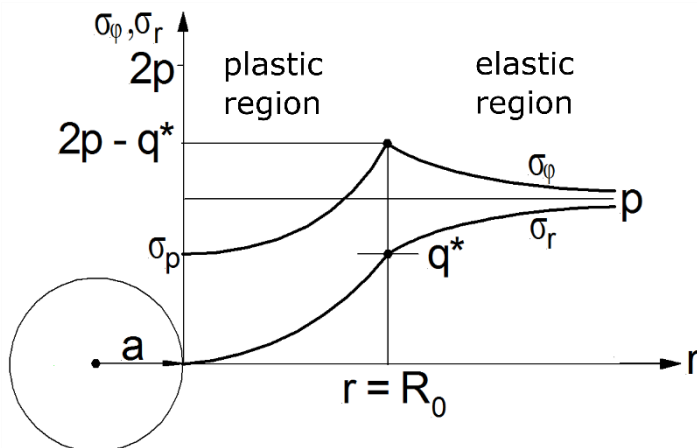

Fig. 16: Stress paths for radial and tangential stress components as function of distance
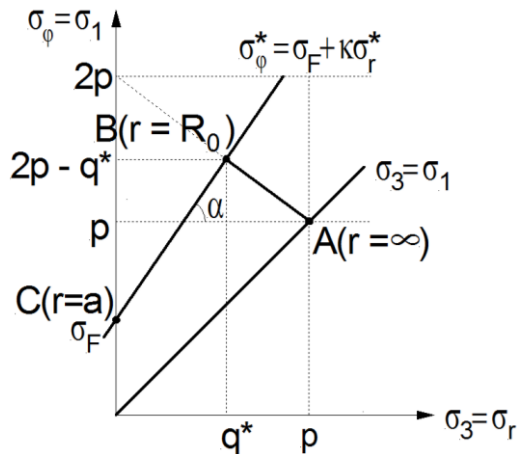
Simple analytical solutions for underground circular, elliptical and rectangular openings

Only for private and internal use!   Updated: 22 February 2022

Fig. 17: Stress values (from A: far-field over B: boundary elastic-plastic region to C: boundary of opening) in principal stress diagram

2.6 Circular inclusion

The problem of 'inclusion' is a fundamental mechanical one in elasticity, but is also of great practical importance for rock mechanics, e.g. the interaction of the lining of bore-holes, shafts or drifts with the surrounding rock mass. Fig. 18 illustrates the problem considering that an inclusion has the shape of a cylindrical shell with inner diameter a and outer diameter b. Rock mass is characterized by Young's modulus E and Poisson's ratio v. The inclusion is characterized by Young's modulus E_0 and Poisson's ratio v_0.

Two different approaches can be followed:

- Considering that rock mass and inclusion exist (1. Phase) and far-field stress is applied afterwards (2. Phase) – primary inclusion.

- Considering that rock mass exist, far-field stress is already applied and corresponding primary deformations have occurred (1. Phase); in a next step (2. Phase) circular opening with radius b is created and radial pressure is applied to boundary to avoid any displacement; in the last step (3. Phase) the inclusion is inserted and at the same time the support pressure is deleted – secondary inclusion.
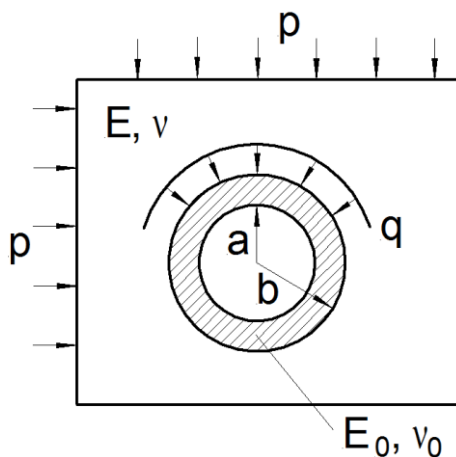

Fig. 18: Cylindrical shell as inclusion inside infinite rock mass under isotropic far-field stress p.

Simple analytical solutions for underground circular, elliptical and rectangular openings

Only for private and internal use!   Updated: 22 February 2022

Elastic solution of this problem is based on the assumption that displacement continuity at the boundary between rock mass and inclusion exist and that normal pressure q acts along the line linking rock mass and inclusion.

2.6.1 Primary inclusion

For the elastic cylindrical shell the following holds for the radial displacement considering plane stress:

$$u_r(b) = \varepsilon_\varphi(b) \cdot b = \frac{1}{E_0}\left[\sigma_\varphi(b) - v_0\sigma_r(b)\right] \tag{44}$$

By substituting the tangential and radial stress components by the expression for thick-walled tubes under inner and outer pressure according to Lame the following expression can be obtained:

$$u_r(b) = \frac{b}{E_0}(m - v_0)q, \tag{45}$$

where $m = \left(b^2 + a^2\right)/\left(b^2 - a^2\right)$.

For the rock mass the following expression holds for the radial displacement:

$$u_r(b) = \frac{b}{E}\left[2p - (1+v)q\right] \tag{46}$$

Equate expression (44) and (46) and solve the equation for q leads to the following expression:

$$q = \frac{2E_0}{E(m - v_0) + E_0(1+v)}p \tag{47}$$

2.6.2 Secondary inclusion

The general procedure is similar to the one explained in Chapter 2.6.1, but the primary displacements have to be subtracted. Therefore, the equivalent expression to 46 is as follows:

$$u_r(b) = \frac{b}{E}\left[2p - (1+v)q\right] - \frac{b(1-v)}{E}p = b\frac{1+v}{E}(p - q) \tag{48}$$

Eq. (48) is set equal to Eq. (45):

$$q = \frac{(1+v)E_0}{E(m - v_0) + E_0(1+v)}p \tag{49}$$

Considering Eq. (47) and (49) the following conclusions can be drawn:

Simple analytical solutions for underground circular, elliptical and rectangular openings

Only for private and internal use!   Updated: 22 February 2022

- $q_{\text{primary}} > q_{\text{secondary}}$
- for secondary inclusion: if $E_0 \to \infty$ or $E \to 0$, then $p = q$
- for primary inclusion: if $E_0 \to \infty$ or $E \to 0$, then $q = 2(1+v)p$
- if $a \to 0$ or $E_0 \to 0$, then $q \to 0$

Primary inclusion is typical for cut-and-cover technology whereas secondary inclusion represents the situation of support in underground mining o tunnelling.

2.6.3 Inclusion and visco-elastic rock mass behaviour

The above mentioned expressions can be extended by considering rheological, that means time-dependent, rock mass behaviour. Using the so-called Volterra or Correspondence Principle, elastic constants have to be replaced by visco-elastic operators. Simplifying Poisson's ratio for rock mass and inclusion are set identical. Under this assumption Young's modulus has to be replaced by the following expressions:

- Kelvin model (parallel connection of spring and dashpot with viscosity η):

$$E \to E\left(1 + \frac{\eta}{E}\frac{\text{d}}{\text{d}t}\right) \tag{50}$$

- Maxwell model (series connection of spring and dashpot with viscosity η):

$$E \to E\left(\frac{\eta\dfrac{\text{d}}{\text{d}t}}{1+\tau\dfrac{\text{d}}{\text{d}t}}\right) \tag{51}$$

Insertion of expressions 50 and 51 into Eq. (49) and assuming that v=0.5 leads to a differential equation for q, which can be solved under consideration of initial conditions, so that the following final expressions can be obtained:

- for Kelvin model:

$$q(t) = \frac{p}{1+\dfrac{2}{3}(m-v_0)\dfrac{E}{E_0}}\left(1 - \text{e}^{-\frac{\alpha}{\tau}t}\right) \tag{52}$$

- for Maxwell model:

$$q(t) = p\left(1 - \text{e}^{\frac{-1}{\left(1+\frac{2}{3}(m-v_0)\frac{E}{E_0}\right)\tau}t}\right) \tag{53}$$

where $\tau = \eta/E$ and $\alpha = \dfrac{1 + \dfrac{2}{3}(m - v_0)\dfrac{E}{E_0}}{\dfrac{2}{3}(m - v_0)\dfrac{E}{E_0}}$.

Both approaches deliver a non-linear q-t-response. For $t \rightarrow \infty$ the following results are obtained:

- for Kelvin model:

$$q = \frac{p}{1 + \dfrac{2}{3}(m - v_0)\dfrac{E}{E_0}} < p \tag{54}$$

- for Maxwell model:

$$p = q \tag{55}$$

2.7 Convergence-Confinement Method

The Convergence-Confinement Methods (CCM) was developed for tunnel dimensioning and consist of two parts:

- the Ground Reaction Curve (GRC)
- the Support Characteristic Curve (SCC)

CCM assumes a circular tunnel under isotropic far-field stress. The rock mass itself is described by either isotropic and homogeneous elastic or isotropic and homogeneous elasto-plastic material behaviour.

The GRC relates the support pressure acting at the tunnel boundary to the radial displacements at the tunnel boundary. The GRC for isotopic linear elastic rock mass response is illustrated in Fig. 19. Radial displacement is zero in case the radial pressure at the tunnel contour q equals the far-field stress p. Radial displacement u increases with decreasing radial pressure until the maximum displacement u_0 is reached for vanishing radial pressure.
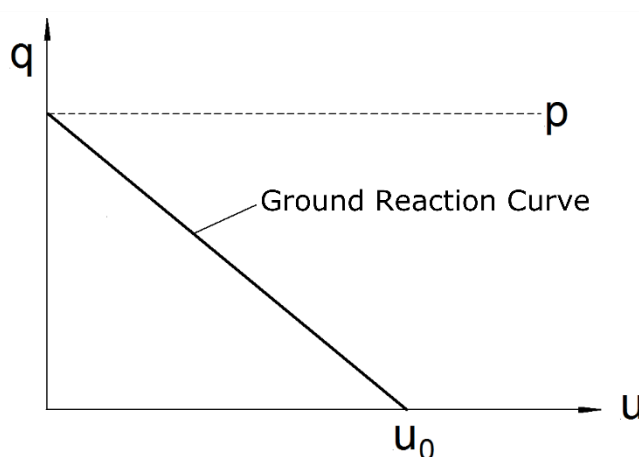

Fig. 19: Ground Reaction Curve for linear elastic rock mass: radial pressure vs. radial displacement.

Simple analytical solutions for underground circular, elliptical and rectangular openings

Only for private and internal use!   Updated: 22 February 2022
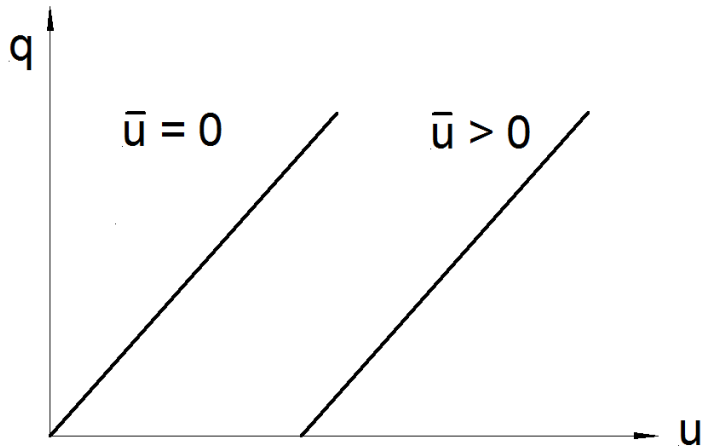

Fig. 20: Support Characteristic Curve for linear elastic support response: support pressure vs. radial displacement.

The SSC describes the bearing pressure due to the convergence of the tunnel. If one again assumes linear elastic response for the support corresponding SCC can be illustrated as shown in Fig. 20. The displacement value $\bar{u}$ describes the initial gap between the tunnel contour and the support and k is the stiffness of the support.

The intersection between GRC and SCC describes the operation point of the system and allows the determination of both, the support load and the tunnel convergence. The working point can be determined by the following equations:

$$u = \frac{q}{k} + \bar{u} \quad \text{for SCC and} \quad q = p - \frac{u}{u_0} p \quad \text{for GRC} \tag{56}$$

Determination of the intersection delivers the following values for the working point:

$$q^* = \frac{k\left(u_0 - \bar{u}\right)}{p + k \cdot u_0} \cdot p \tag{57}$$

$$u^* = \left(1 - \frac{k\left(u_0 - \bar{u}\right)}{p + ku_0}\right) u_0 \tag{58}$$

Simple analytical solutions for underground circular, elliptical and rectangular openings

Only for private and internal use!   Updated: 22 February 2022
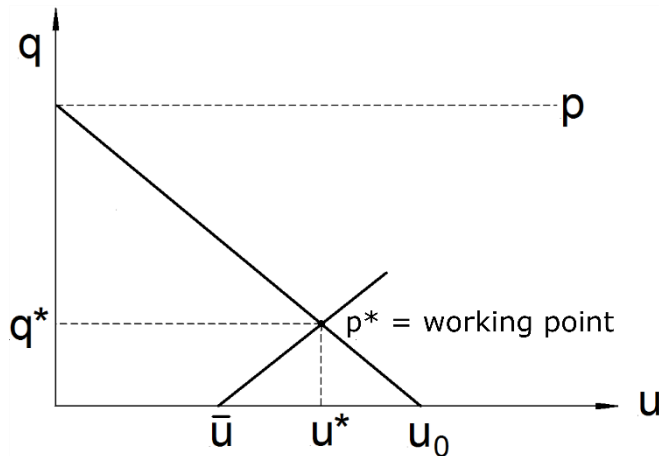

Fig. 21: Illustration of working point as intersection of GRC and SCC for linear elastic material response of rock mass and support.
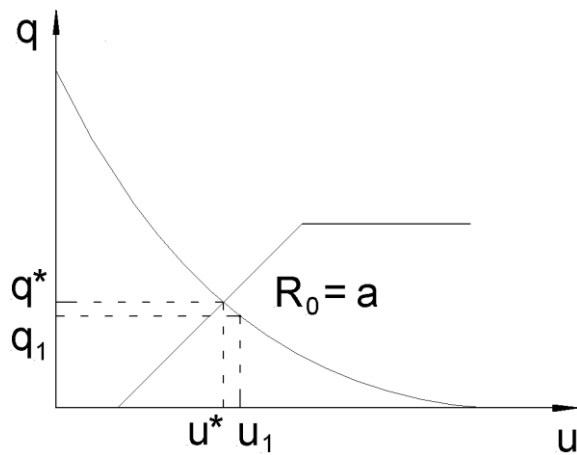

Fig. 22: Illustration of interaction between GRC and SCC in case of nonlinear behavior

Fig. 21 shows that bearing pressure of the support increases with increasing stiffness of the support, reduced gap between support and tunnel contour and decreasing stiffness of the rock mass and vice versa.

Considerations regarding GRC and SCC can be extended by including nonlinear behaviour for rock mass and support. Typical curve progression is shown in Fig. 22. Support is represented by elastic – prefect plastic behaviour. Rock mass is represented by elasto-plastic behaviour according to Mohr-Coulomb theory. Plastic rock mass behaviour starts, whenever the extension of the plastic zone reaches the radius of the opening ($R_0 = a$, where $q = q_1$ and $u = u_1$)

Extending the solution given in chapter 2.5 one can show which support pressure q would be necessary to avoid the development of a plastified zone. The radial pressure inside the plastified zone under action of internal pressure q is given as follows:

$$\sigma_r{}^* = \frac{\sigma_F}{\chi - 1}\left[\left(\frac{r}{a}\right)^{\chi-1} - 1\right] + q\left(\frac{r}{a}\right)^{\chi-1} \tag{59}$$

According to the Mohr-Coulomb failure criterion (34) at the transition between elastic and plastic region the radial stress is defined as:

$$\sigma_r{}^*(R_0) = \frac{2p - \sigma_F}{\chi + 1} \tag{60}$$

Equalizing (59) and (60) for r = R₀ allows to determine the radius of the plastic zone under consideration of supporting pressure q:

$$\frac{R_0}{a} = \sqrt[\chi-1]{\frac{(\chi-1)(2p-\sigma_F) + \sigma_F(\chi+1)}{(\chi+1)(\sigma_F + q(\chi-1))}} \tag{61}$$

Plastification of a rock mass starts whenever the following condition holds $(R_0 \geq a)$:

$$q > \frac{2p - \sigma_F}{\chi + 1} \tag{62}$$

A more general solution considering non-linear Hoek-Brown failure criterion is given by Carranza-Torres & Fairhurst (2000). Further comments are given for example by Kainrath-Reumayer et al. (2009) and Oreste (2009).

Simple and easy to handle software tools were developed like 'Rocksupport' (2015). Such tools allow to consider nonlinearities of rock mass and support. They also deliver data sets to convert support effects of anchors, shotcrete etc. into equivalent support pressure q.

Fig. 23 illustrates different potential constellations of interaction between rock mass and support. This diagram shows, how stiffness and installation time or gap between support and rock mass influence the arch forming.

Simple analytical solutions for underground circular, elliptical and rectangular openings

Only for private and internal use!   Updated: 22 February 2022

Fig. 23: Illustration of potential interaction of GRC with different SCC

2.8   Rectangular opening in infinite elastic space

For openings with rectangular cross section only approximate analytical solutions exist like compiled by Denkhaus (1958). In these approximate solutions the rectangular cross section is considered as a special case of an ellipse by using rectilinear coordinates, which delivers rectangular cross sections with rounded corners.

For an opening with quadratic cross section under isotropic far-field stress the tangential stress at the contour σ_θ can be expressed by the following formula (see also Fig. 24):

$$\sigma_\Theta = p \left[\frac{2\left(1-9n^2\right)}{1+9n^2 - 6n \cdot \cos(4\Theta)} \right] \tag{63}$$

Simple analytical solutions for underground circular, elliptical and rectangular openings

Only for private and internal use!   Updated: 22 February 2022

where:

        σ_Θ = tangential stress at the surface
        p = in-situ far-field stress
        n = factor describing the sharpness of the corner (see Fig. 24)
        Θ = angle according to Fig. 24

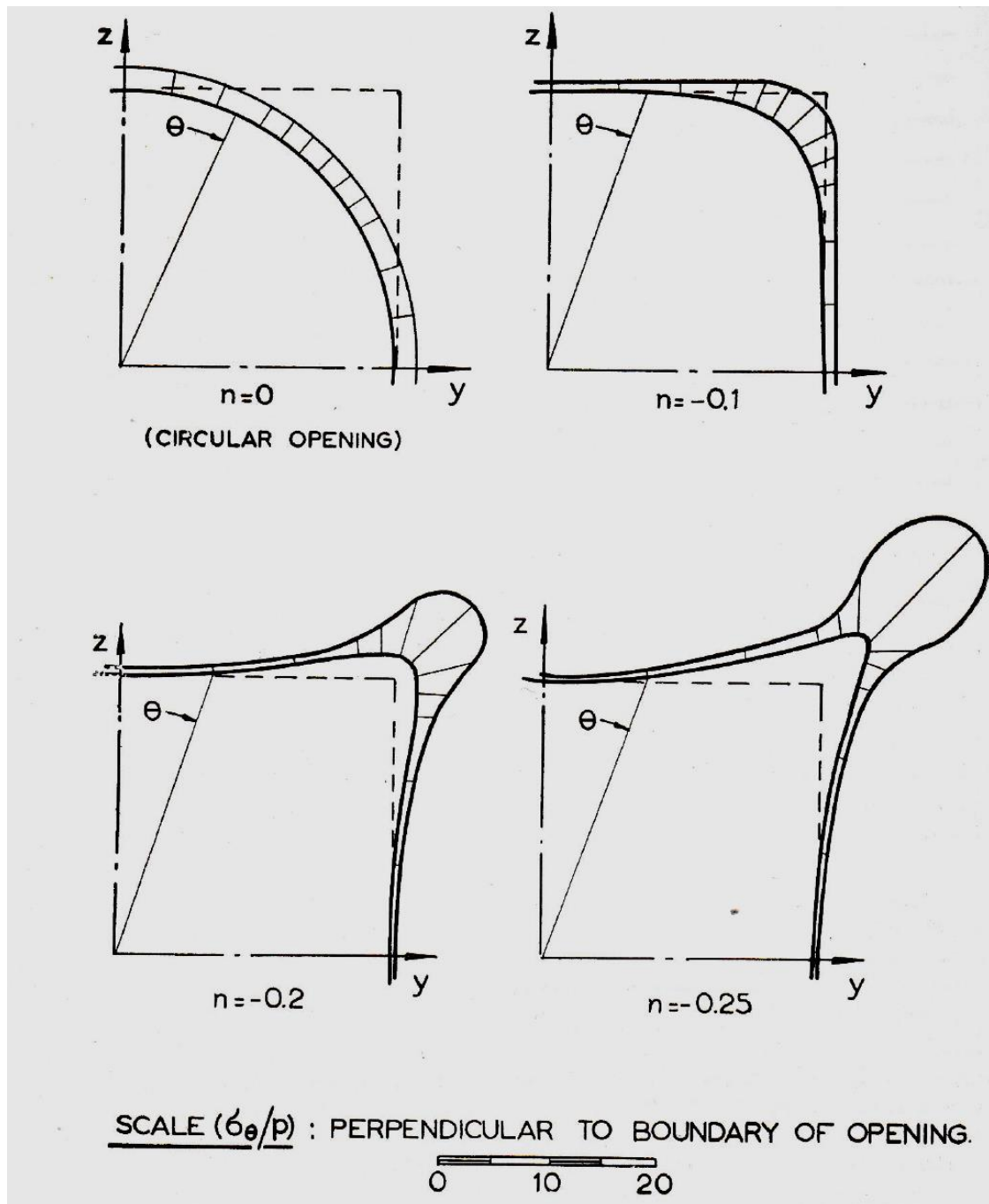Note: best approximation for the square are reached for values of n between -0.100 and 0.111 (see Fig. 24).

Fig. 24: Scaled tangential stress at the contour of a quadratic opening under isotropic far-field stress p for different values of n according to Eq. 63 (Denkhaus, 1958).
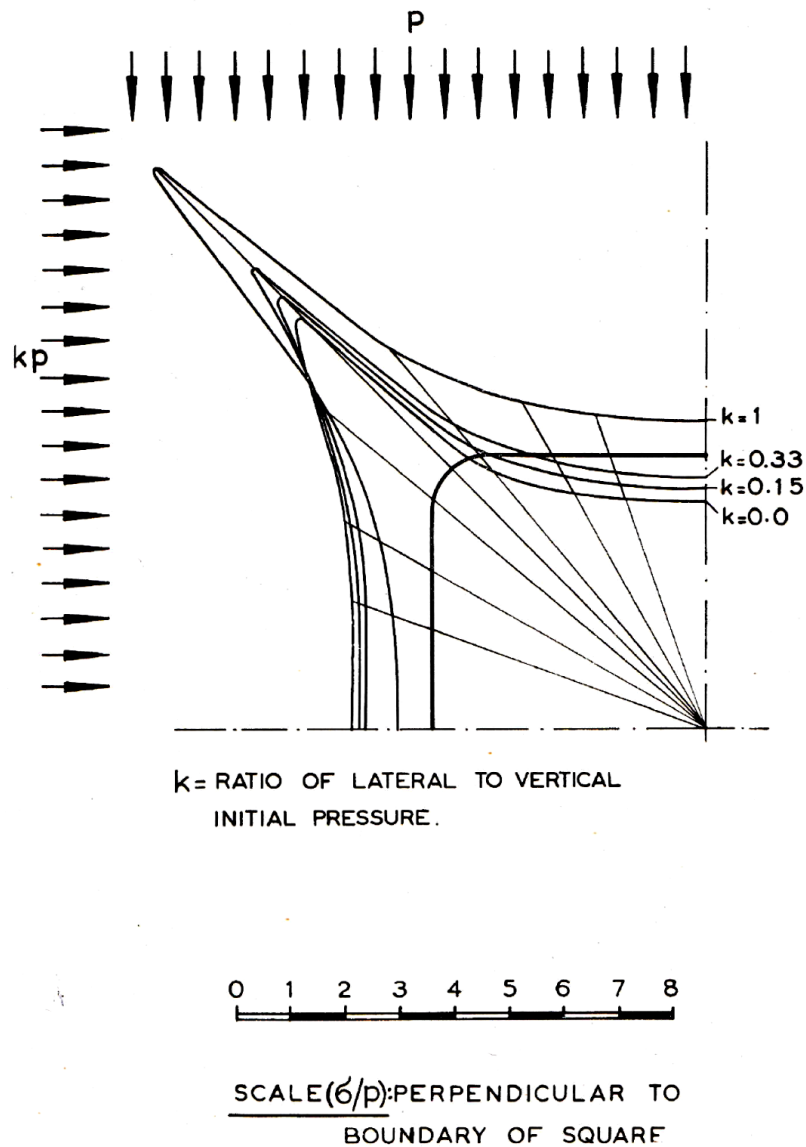
Fig. 25: Scaled tangential stress at the contour of a quadratic opening under anisotropic far-field stresses p and k·p for different values of k (Denkhaus, 1958).

The following formula describes the tangential stress concentration at the contour for an opening with a rectangular cross section with different height to width ratio exposed to an isotropic far-field stress:

$$\sigma_\Theta = p \left[\frac{2}{1-n} \cdot \frac{(1-n)(1-9n^2) - m^2(1+n) + 4mn \cdot \cos(2\Theta)}{1+m^2+9n^2 - 2m \cdot (3n-1) \cdot \cos(2\Theta) - 6n \cdot \cos(4\Theta)} \right] \tag{64}$$

with:

$$m = (1+n)\frac{\left(\dfrac{c}{b}-1\right)}{\left(\dfrac{c}{b}+1\right)} \tag{65}$$

where:

σ_Θ = tangential stress at the surface
p = in-situ far-field stress
n = factor describing the sharpness of the corner (see Fig. 24)
Θ = angle according to Fig. 24
c = width of opening
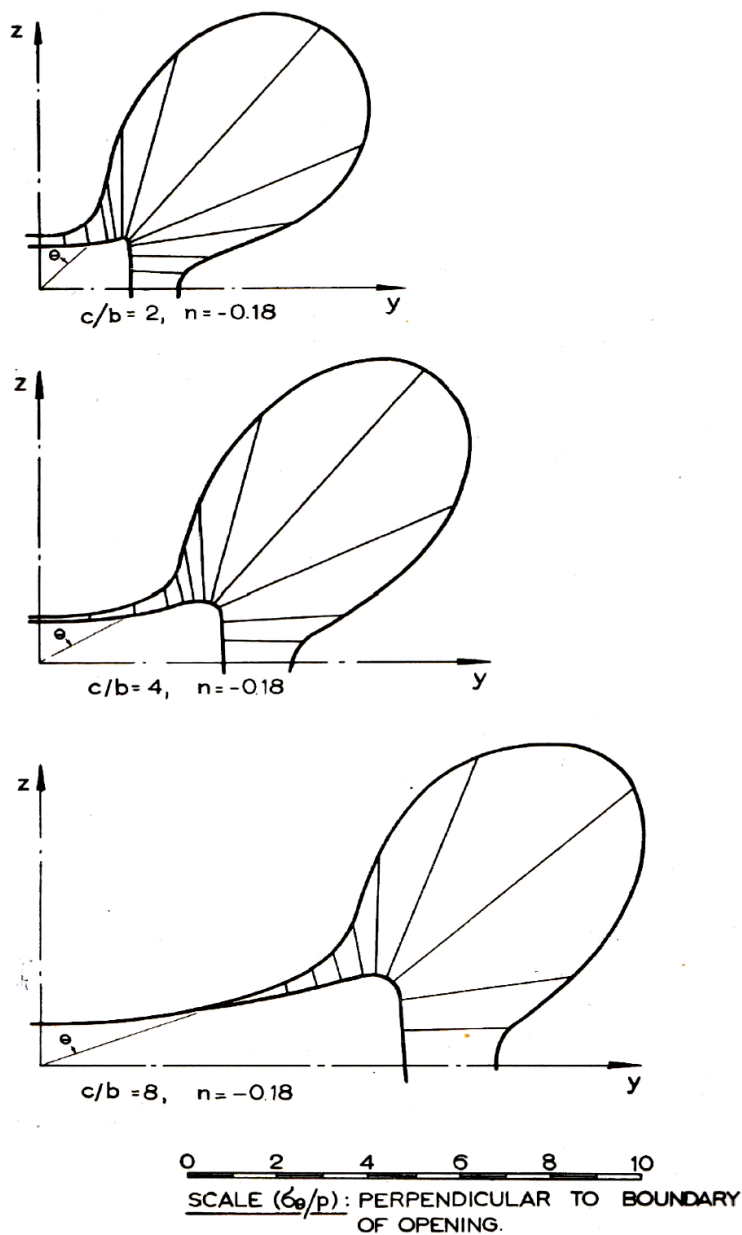b = height of opening

Fig. 26: Scaled tangential stress at the contour of a rectangular opening with width c and height d under isotropic far-field stress p (Denkhaus, 1958).

Similar results are given by Heller et al. (1959) as shown in Fig. 26 in terms of stress amplification (maximum tangential stress at boundary to initial isotropic stress) for different values of K (ratio of height to width of rectangular opening) and different values of ρ (ratio of corner radius to smaller edge length of opening).
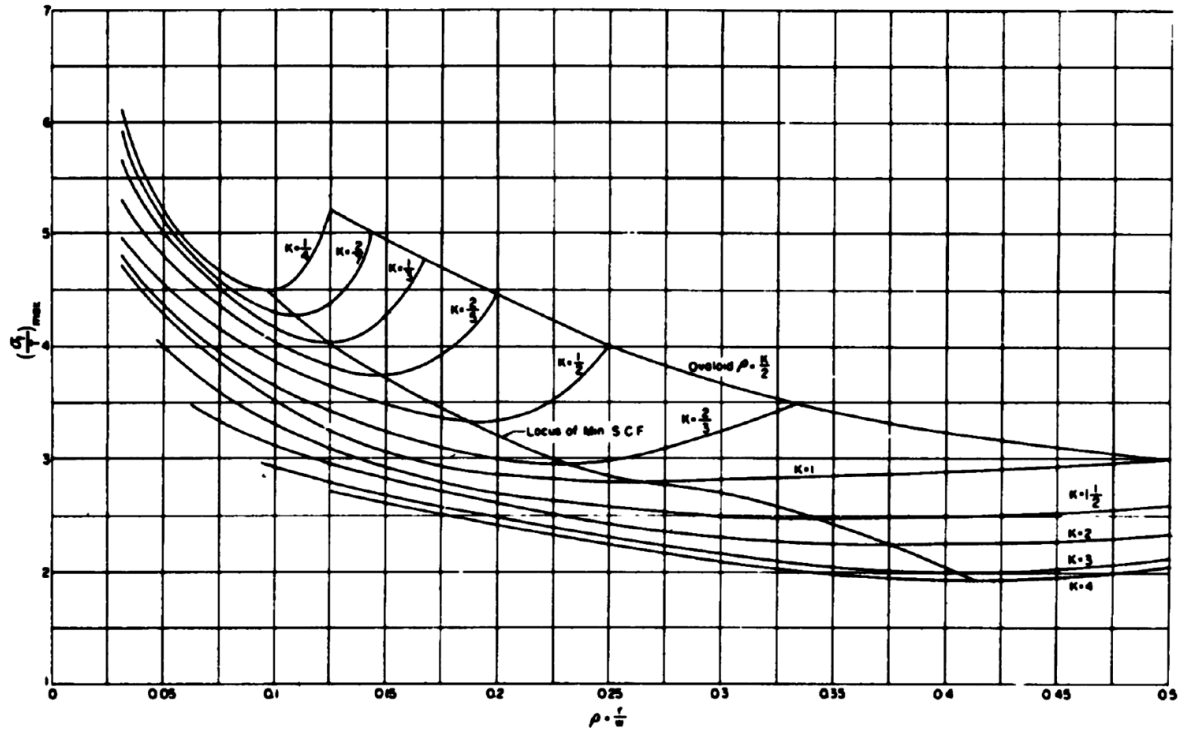

Fig. 27: Stress concentration factor at contour as function of radius ratio ρ (corner radius / smaller edge length of opening) for rectangular opening with K-ratio (width to height ratio of opening) under isotropic far-field stress (Heller et al., 1959).

As Fig. 27 indicates: the sharper the edge, the stronger the stress concentration. However, the increase is non-linear and becomes weaker with increasing sharpness of the edge. As illustrated also in Fig. 28, the rounding of corners in-situ will lead to realistic local stress magnification up to about 5, but definitely not exceed 10.
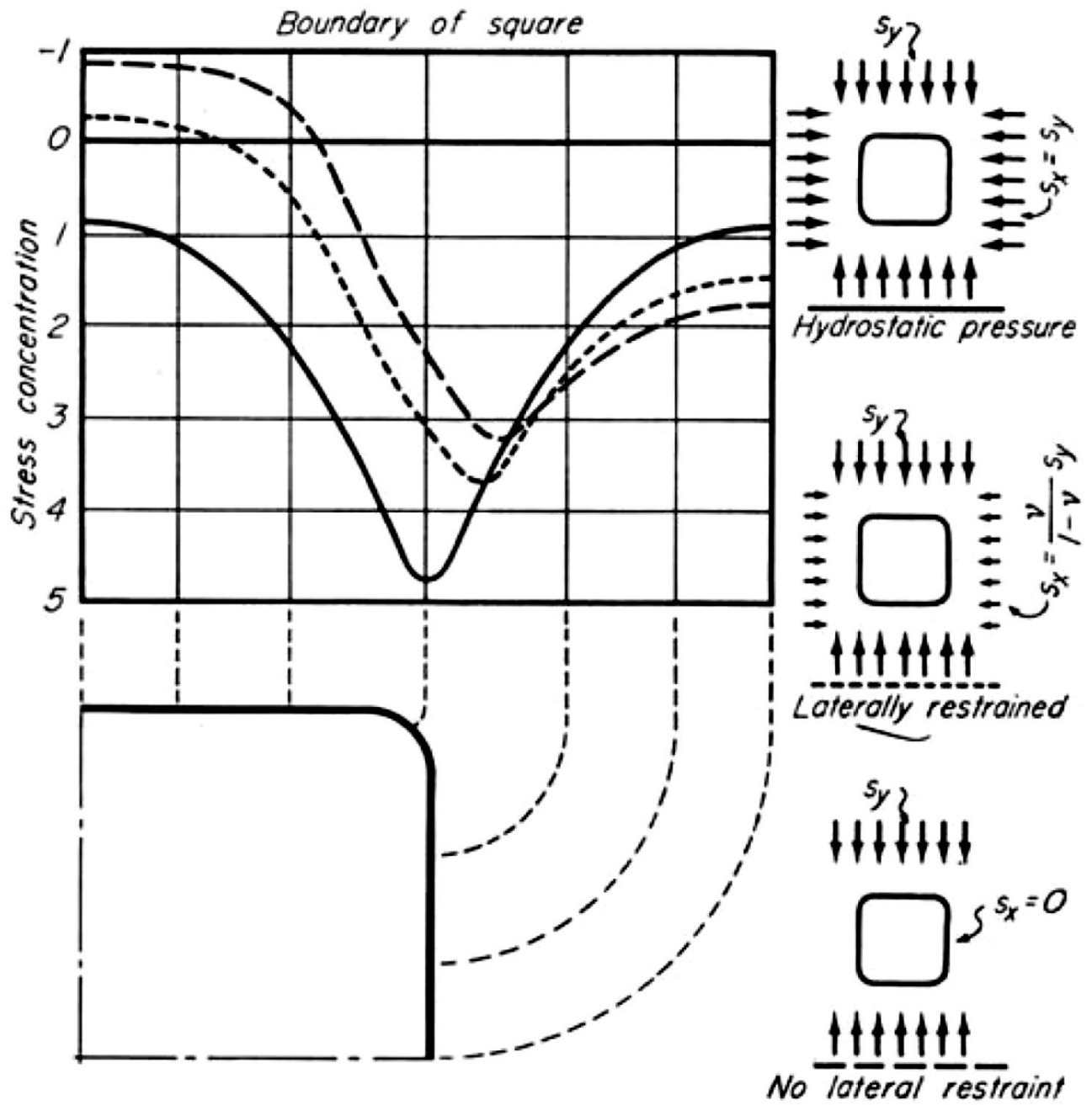
Fig. 28: Stress concentration factor at contour as function of far-field stress ratio for quadratic opening (corner radius / length of opening = 1/12) (Caudle & Clark, 1955).

3 Wellbore stability

In respect to wellbore stability two problems have to be considered: potential borehole breakouts (shear failure) and potential hydraulic fracturing (tensile frailure). By extending the classical Kirsch solution (see chapter 2) and considering pore water pressure, wellbore mud pressure and thermal stresses the following critical stresses can be found at the borehole wall:

$$\sigma_\varphi^{min} = 3S_h - S_H - 2P_p - \Delta P - \sigma_\varphi^{term} \tag{66}$$

$$\sigma_\varphi^{max} = 3S_H - S_h - 2P_p - \Delta P - \sigma_\varphi^{term} \tag{67}$$

$$\sigma_\varphi^{term} = \frac{\alpha \cdot E \cdot \Delta T}{1 - \nu} \tag{68}$$

where:

σ_φ^{min} minimum effective tangential stress at borehole wall
σ_φ^{max} maximum effective tangential stress at borehole wall
S_h minimum primary (virgin) principal horizontal stress
S_H maximum primary (virgin) principal horizontal stress
P_p Pore water pressure
σ_φ^{term} Thermal tangential stress at borehole wall
ΔP Difference between borehole pressure (mud weight) and pore water pressure
UTS Uniaxial tensile strength
UCS Uniaxial compressive strength
E Young's modulus
ν Poisson's ratio
ΔT Temperature difference
α Thermal expansion coefficient

Borehole damage has to be considered under the following circumstances:

if $\sigma_\varphi^{min} < UTS$ hydraulic fracturing   (69)

if $\sigma_\varphi^{max} > UCS$ borehole breakout   (70)

Eq. 69 and 70 consider the problem in a simplified manner (uniaxial). Especially for the initiation of borehole breakouts the assumption of the Mohr-Coulomb criterion may provide more precise results:

$$0 = \sigma_\varphi^{max} - \frac{1 + \sin\phi}{1 - \sin\phi} \Delta P - \frac{2c\cos\phi}{1 - \sin\phi} \tag{70}$$

4 Literature

Aednoy, B.S. & Looyeh, R. (2011): Petroleum rock mechanics, Gulf Professional Publishing, 350 p.

Carranza-Torres, C. & Fairhurst, C. (2000): Application of the convergence-confine ment method of tunnel design to rock masses that satisfy the Hoek-Brown failure criterion, Tunneling and Underground Space Technology, 15: 187-213

Caudle, R.D. & Clark, G.B. (1955): Stresses around mine openings in some simple geologic structures, University of Illinois Bulletin No. 430

Denkhaus, H.G. (1958): The application of the mathematical theory of elasticity to problems of stress in hard rock at great depth, The Association of Mine Managers of South Africa,1958/59: 271-310

Heller, S.R. et al. (1959): The stress around a rectangular opening with rounded corners in an uniformly loaded plate, Department of the navy, structural mechanics laboratory, report 1290

Hudson, J.A. (Ed.), (1993): Comprehensive rock engineering, Pergamon Press, Vol. 1-5

Jaeger, J.C. et al. (2007): Fundamentals of rock mechanics, Blackwell Publishing, 475 p.

Kainrath-Reumayer, S. (2009): The convergence confinement method as an aid in the design of deep tunnels, Geomechanics and Tunneling, 2(5): 553-560

Obert, L. & Duvall, W.I. (1967): Rock mechanics and the design of structures in rock, John Wiley & Sons, 650 p.

Oreste, P. (2009): The convergence-confinement method: roles and limits in modern geomechanical tunnel design, American J. of Applied Sciences, 6(4): 757-771

Pariseau, W.G. (2007): Design analysis in rock mechanics, Taylor & Francis, 560 p.

Rocksupport (2015): https://rocscience.com/rocscience/products/rocsupport

Taheri, Z. (2004): Führer durch die räumliche Elastizitätstheorie, ICONEON, 159 p.